Design and control of a new electrostrictive polymer based continuum actuator for endoscopic robot

Q.JACQUEMIN[1], Q.SUN[2], D.THUAU[2], E.MONTEIRO[1], S.TENCE-GIRAULT[1,3], S.DOIZI[4], O.TRAXER[4] and N.MECHBAL[1]*

Abstract

Minimally Invasive Surgery (MIS) consists of the insertion of a flexible endoscope into the patient body through natural orifices. Over the past few decades, the growing interest in microelectromechanical systems (MEMS) has paved the way for ubiquitous miniaturized integrated sensors and actuators in medical endoscopy. Nowadays, recent advances in materials have opened a promising way to fulfill the surgical requirements and size constraint for the development of smart continuum structures. Among smart materials, electroactive polymers (EAPs) exhibit exceptionally large, fast, repeatable, and reversible motions while perfectly meeting the requirements of micro-integration. However the high applied voltage required for the actuation is not compatible with in vivo medical application. To overcome these issues, a multilayered concept has been proposed. In this work a relaxor ferroelectric electrostrictive polymer is studied for its large electromechanical strain. A wide range of parameters involved in the active material has led us to the development of a finite element model on Abaqus to guide the experimental development. Then, to control this smart endoscopic robot a kinematic and a dynamic models have been built. To test and validate these

*[1]Laboratoire PIMM, Arts et Metiers Institute of Technology, CNRS, Cnam, HESAM Universite, 151 Boulevard de l'Hopital, 75013 Paris, France

†[2]Laboratoire de l'Integration du Materiau au Systeme (IMS, UMR 5218) 351 Cours de la Liberation, 33400 Talence, Cedex, France.

‡[3]Arkema, CERDATO, Route du Rilsan, 27470 Serquigny, France

§[4]Hôpital Universitaire de Tenon, 4 Rue de la Chine, 75020 Paris, France

models a Co-simulation procedure has been developed. This procedure coupled Abaqus and Matlab-Simulink allowing testing proposed control algorithms.

1 Introduction

The development of microscale sensors and actuators has improved the quality of surgical tools. Optical cameras, essential to endoscopy based diagnostic, have been miniaturized to the point that they can be embedded in tools a few millimeters in diameter.

Furthermore, smart materials and among them electroactive polymers that have the ability to bend under the effect of an electric field Lheritier et al. (2020) have been largely integrated into soft actuators structures. This has led to continuous soft actuators with unconventional electromechanical properties representing ideal candidate for a novel generation of soft endoscopic robotics. These soft actuators offer an unequalled dexterity enabling the realization of very complex tasks in microsurgery while reducing the invasiveness of endoscopic tools Bar-Cohen (2004*a*), Bar-Cohen (2004*b*) and Cho et al. (2016). Guided by the surgical need for reversible and repeatable motion with high deformation and precision, we focused our study on a ferroelectric relaxor terpolymer, namely poly(vinylidene fluoride-trifluoroethylene-chlorotrifluoroethylene), P(VDF-*ter*-TrFE-*ter*-CTFE) that shows a high electrostrictive strain, i.e., the ability to produce a large field-induced strain when exposed to an external electric field. In the pursuit of designing soft actuators exhibiting large deformation at reduced applied voltage, this study proposes a multilayer electrostrictive actuator presenting excellent electromechanical performances under an applied voltage divided by the number of layers. In particular, this work investigates the impacts of material properties, actuator geometry and manufacturing parameters on the actuator performances in order to elucidate the design specifications to conceive soft actuators that fulfill medical endoscopic soft robotics requirements. Despites few available studies on multilayered composite have been reported based on diverse dielectric elastomers Duduta et al. (2016), Kadooka et al. (2015),Balakrisnan et al. (2015) and O'Brien et al. (2008) but also using electrostritive polymers Ahmed et al. (2017), Ahmed & Billah (2016), McGough et al. (2014), Frecker & Aguilera (2004), and Capsal et al. (2015), those are limited

to the experimental proof of concept.

Herein, we further implemented a modeling theory for accurate control of an electrostrictive continuous soft actuator validated virtually through a numerical co-simulation implemented simultaneously on Matlab, Simulink and Abaqus software. From now on, the electrostrictive polymer material used in this paper will be refered as ESP for ElectroStrictive Polymer.

2 Mechanical behaviour of the ESP actuator

The electrostriction phenomenon is described by the following electromechanical equations:

$$\begin{cases} S = s^E T + E^t M E \\ D = \varepsilon^T E + 2T^t M E \end{cases} \tag{1}$$

With S the strain tensor of the material and T the stress tensor. s^E and ε^T are respectively the elastic coefficient at constant electric field and the electric permittivity at constant stress while E represents the electric field. M is the matrix of the electrostrictive coefficients and D symbolizes the electric displacement with $Q = \int_s D ds$ where Q represents the amount of electric charge contained in a volume delimited by the surface s. Equation 1 describes the electromechanical operation of electrostrictive materials. The strain is a function of a quadratic form of the electric field and the dimensions of the material are modified in the directions perpendicular to the electric field. It is only when the ESP is associated with a passive material called substrate that the elongation phenomenon is constrained and thus results in an asymmetrical deformation of the bending type as presented in figure 1a. On this same figure we observe that the active material is surrounded by electrodes on both sides and $r = 1/k$ represents the radius of curvature. The composition and thickness of the substrate and electrode layers play a key role in the performance of the actuator. In order to increase the bending and the force induced by the system, it is then possible to multiply the number of active material layers, here the ESP. This type of actuator is called a multilayer (figure 1b). Although theoretical studies on multilayers have demonstrated their benefits, the experimental realization is very complex, especially given that the layers of material are in the order of a few microns.

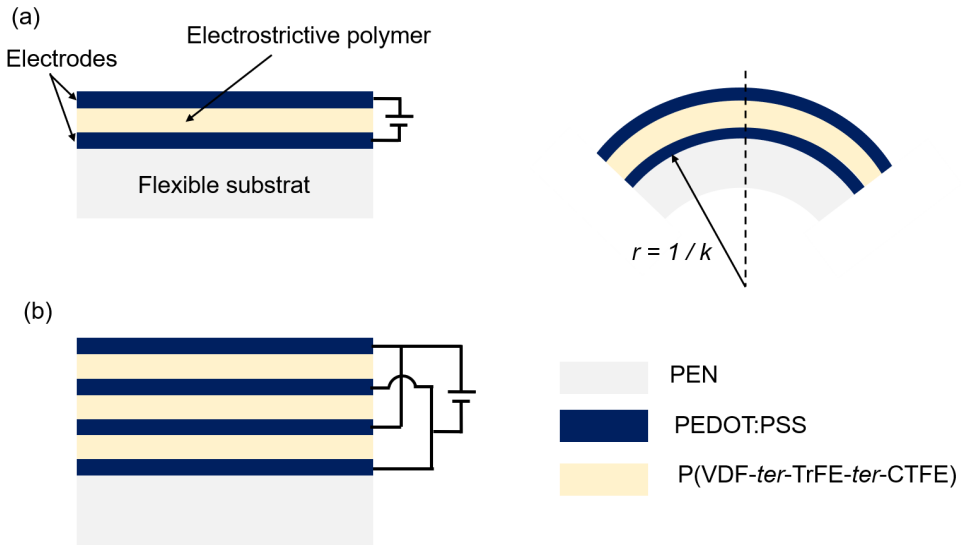

Figure 1: a) Schematic of the composite material with the different materials and its curvature b) Schematic of the multilayer composite material

2.1 Numerical analysis

The analytical description of the composite actuator can be modeled on a numerical software through the finite element method. In this study we will perform a quasi-static analysis of a composite beam. We will then study the resisting force of this beam in front of an obstacle which lead us to the expression of the force induced by the actuator.

Thus, the finite element model of the actuator was developed on the Abaqus software of Dassault Systèmes®. Unlike piezoelectric materials, the behavior of electrostrictive materials is not directly implemented in this software. We have therefore simulated the propagation of a non-linear electric field in the electrostrictive material through a thermal analogy Hsueh (2002), Pandya & Kant (1988) and Kant et al. (1992). The model is made of shell elements in order to counteract the imbalance between the thickness and length of the actuator since the ratio between the two is $r \approx \frac{1}{1000}$. It is geometrically nonlinear and configured for large displacements and small deformations. Some characteristic dimensions of the system being of the order of the hundred of nanometers, a conversion in SI(mm) is implemented on the model

to avoid being confronted with the zero of the numerical calculation software.

The numerical study evaluates the influence of the parameters on the bending power and on the force induced by the actuator. Figure 2a presents the bending of the actuator with $\theta = 90^{circ}$.

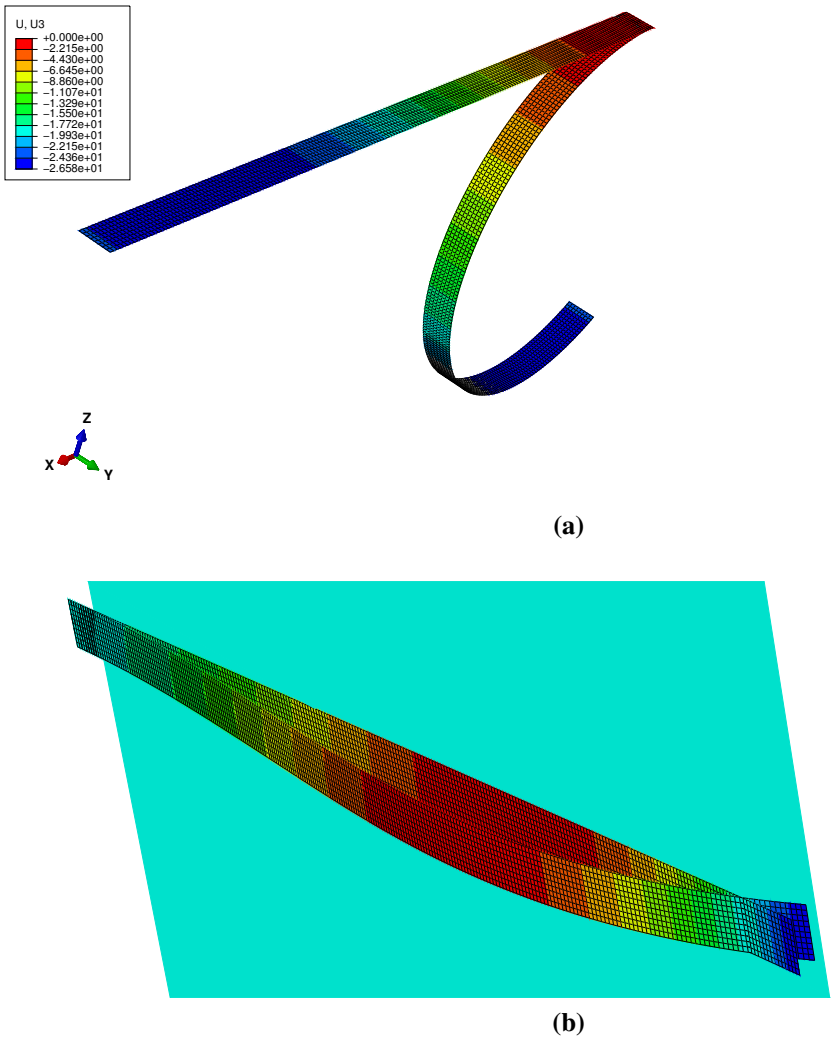

Figure 2: a) Flexion of the composite actuator subjected to an electrostrictive field and b) Numerical model on Abaqus software of the actuator in contact with a fixed plane

Figure 2b presents the simulation model that will be used to study the contact force between the actuator and a fixed plane. This contact force allows the evaluation of the force induced by the actuator. We can thus observe in figure 3 the bending capacities of the actuator under the effect of an electric field of $50V/\mu m$. The study then focuses on the influence of Young's

modulus, thicknesses and number of layers.

Thus, figure 3a highlights the influence of the number of layers and the thickness of the ESP. We observe that the system reaches its best performance with few layers and low thickness. Figure 3b shows us that the Young's modulus of the electrodes must be chosen as low as possible, which is confirmed by figure 3d; this is also valid for the thickness of the electrodes. The passive substrate can have a Young's modulus of up to a few giga pascals, provided that the thicknesses remain below $30\mu m$ as shown in figure 3c. This characteristic is constraining since it is the thickness of the substrate material that gives the actuator its stiffness and vacuum resistance.

Moreover, on figure 4c, we observe that concerning the force induced by the actuator, it is at $23\mu m$ that the system is the most efficient whatever the values of Young's modulus observed, provided that they are not too low as shown in figure 4b. It is thus a question of finding a compromise between force and bending by fixing the thickness of the substrate around this value of $20\mu m$ while using a material with a high Young's modulus since this parameter seems to favor bending as well as the induced force. However, figure 3c shows that too high a modulus will eventually stress the system. Figure 4a shows the cross interdependence between the number of layers and the ESP thickness to generate the induced force. This time, the system tends to a larger thickness to generate the force, either by the number of layers or the ESP thickness. However, beyond certain values, a thick ESP does not coincide with too many layers. Both the substrate and the ESP are compatible with a high Young's modulus to generate an induced force as shown in figure 4b and finally, as it was already the case for bending, the electrodes should be chosen thin and with a low Young's modulus.

To sum up this study the system tends towards a larger thickness to generate force, either through the number of layers or the ESP thickness. However, beyond certain values, a thick ESP does not coincide with a satisfying bending capacity. Both the substrate and the ESP are compatible with high Young's modulus to generate induced force and finally, as it was already the case for the bending, the electrodes must be chosen thin and with low Young's modulus.

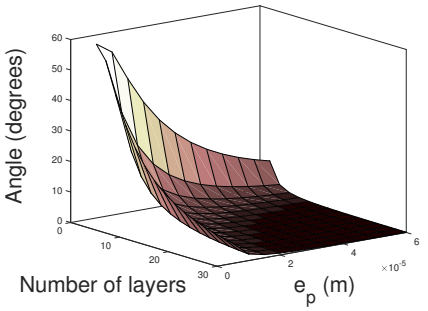

(a)

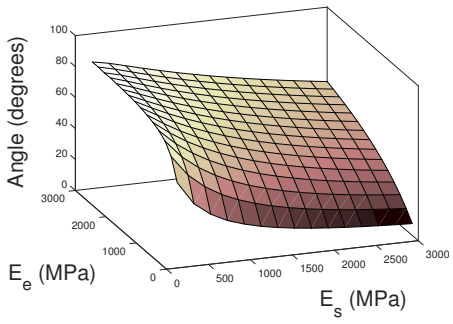

(b)

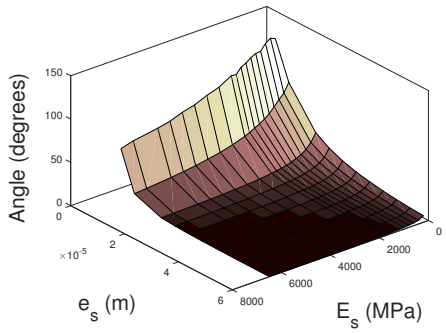

(c)

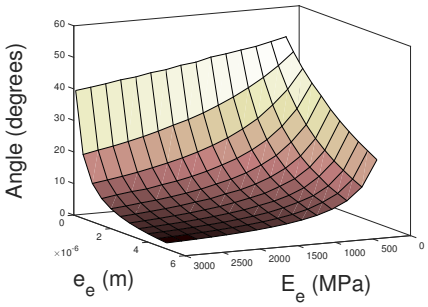

(d)

Figure 3: Simulation result that highlights the bending capabilities of the actuator as a function of the following parameters: a) the number of active layers n and the thickness of the ESP layers e_p b) the Young's modulus of the passive substrate E_s and the Young's modulus of the active material E_p c) the Young's modulus of the passive substrate E_s and its thickness e_s and d) the Young's modulus of the electrode material E_e and its thickness e_e.

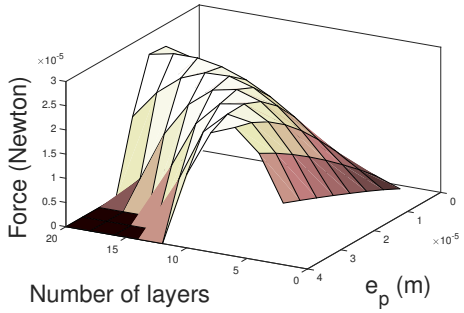

(a)

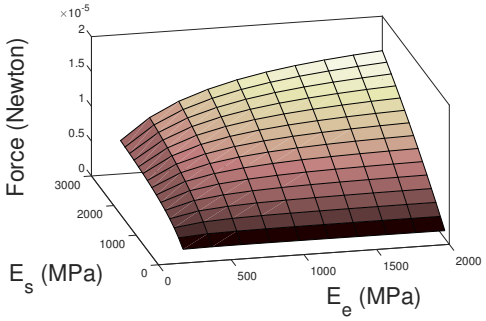

(b)

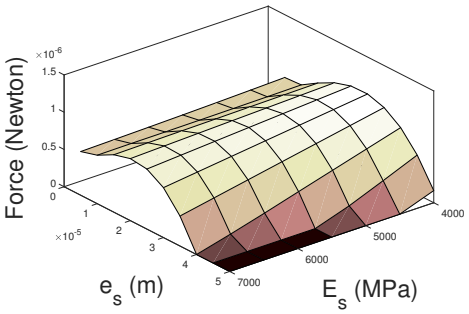

(c)

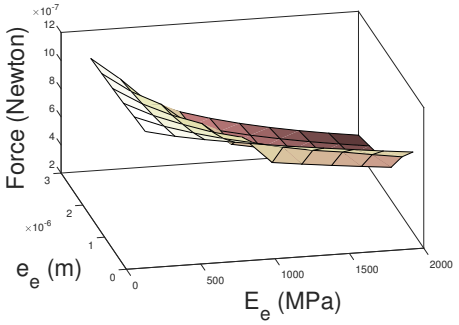

(d)

Figure 4: Simulation result that highlights the induced force capabilities of the actuator as a function of the following parameters: a) the number of active layers n and the thickness of the ESP layers e_p b) the Young's modulus of the passive substrate E_s and the Young's modulus of the electrode material E_p c) the Young's modulus of the passive substrate E_s and the thickness of the passive substrate e_s d) the Young's modulus of the electrode material E_e and the thickness of the passive substrate e_e.

2.2 Experimental analysis

The ESP material used for these experiments is the terpolymer P(VDF-*ter*-TrFE-*ter*-CTFE), with 8.5% mol of CTFE, provided by Piezotech S.A.S (Arkema group, France). It is presented as a powder or as a solution with a solvent in the form of an ink. The viscosity of these inks is variable, it can be adapted to the various printing techniques to target specific thickness of the layers. We conducted an experiment to obtain the breakdown field and it was located around $280V/\mu m$. The breakdown threshold depends on the quality of the printed layers and it is related to the air bubbles or impurities during the manufacturing phase.

Figure 5a depicts the fabrication process flow of the actuators. Initially, a 200 nm thick of conductive polymer PEDOT:PSS was deposited by screen printing with a squeegee speed of 80mm/s applying a force of 120N (step 1). The as deposited layer was then annealed at at 110°C for 10 minutes (step 2). Then, 2 µm thick P(VDF-*ter*-TrFE-*ter*-CTFE) were screen printed at 50mm/s and 100N (step 3) and annealed at 80°C for 5 minutes and subsequently at 110°C for 10 minutes (step 4). The upper electrode was deposited by in the same condition as the bottom electrode (step 5 and 6). For multilayer devices, the different steps of the process were repeated. Table 1 summarizes the characteristics of the materials of the system. A

Table 1: Actuator parameters table

Components	Material	Young's Modules	Thickness
Substrate	PEN	5.5 GPa	25 μm
Electrode	PEDOT-PSS	0.9 GPa	200 nm
ESP	P(VDF-*ter*-TrFE-*ter*-CTFE)	0.2 GPa	2-30 μm
Electrode	PEDOT-PSS	0.9 GPa	200 nm

first experiment consisted in comparing the behavior of the actuator with a similar parametric model from the numerical experiment using the finite element method. Figure 5b presents the results of this test. In particular, it is observed that the trend of the bending angle is similar on both models. However, the radius of curvature of the experimental actuator is not perfectly constant and this likely comes from structural imperfections and edge effect since the actuators are hand-cut from the printed batch. We also noted the reversibility and

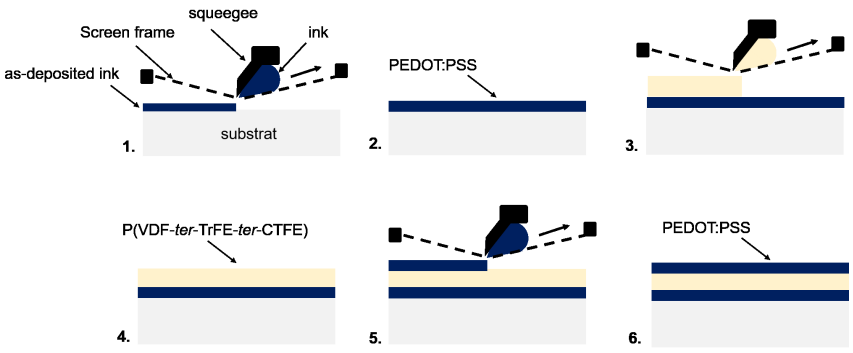

(a)

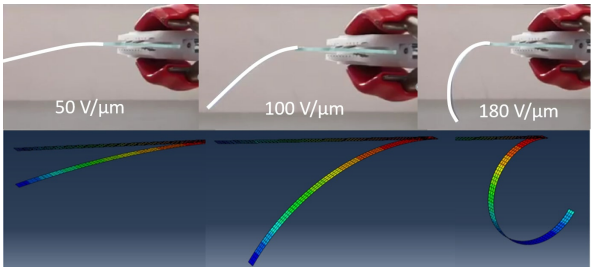

(b)

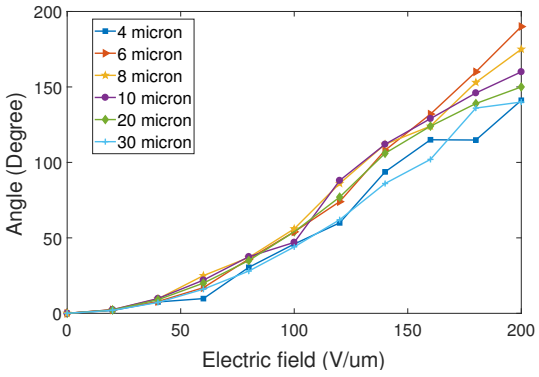

(c)

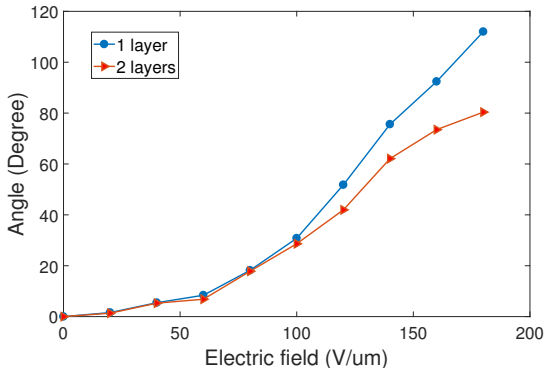

(d)

Figure 5: a) Illustrations of the screen printing process for the actuator design b) comparative results between the experimentation and the theoretical study resulting from the numerical calculation by the finite element method and c) experimental results for different ESP layer thicknesses and d) for different layers

repeatability of the actuation since the material returned to its original shape when the electric field transmission stopped and was also able to reproduce the same trajectory several times under similar voltages. The repeatability was then limited by the deterioration of the material since the small imperfections become a current bridge between the layers and eventually lead to a partial and then to a total degradation of the actuator after about ten handling cycles. Moreover, the precision seemed conclusive at first sight and could be quantified at a few angle degrees although its measurement was noisy due to the imperfections of the prototypes and the dynamics of the system. The induced force was measured around $300\mu N$ for a field up to $125V/\mu m$. The force measurement was performed using a force capacitive sensor from Aurora Scientific. New tests were then carried out by evaluating the variation of the thickness of the ESP layer (figure 5c). The angle measurement was obtained by superimposing the actuator with an angle plotter. This was repeated several times depending on the level of breakdown in the actuator. In order to keep the measurement, it is imperative that the actuator can return to its original position without irreversible deformation. Then the average of the measurements made on the successful experiments is kept to be reported in the results of figures 5 c and d. We observe that globally, the increase of the material thickness is contradictory with the achievement of a high bending. This result coincides with the predictions of the finite element model. However, this trend is only evident at electric fields of $180V/\mu m$ under the experimental conditions. Given the possible positive impact on the induced force and better short circuit resistance of a thick layer, the realization of ESP layers of a few tens of microns is conceivable.

A bilayer prototype actuator was successfully realized by this process. A $20\mu m$ thick bilayer have been printed and compared with a single layer based actuator on figure 5d. It is observed that the batch made up of two layers of ESP is a bit less efficient in terms of bending although it holds its position. This can be explained by the damages caused in the ESP layers. Indeed the bilayer, having undergone more annealing and contact with solvents during the printing phases, degrades more quickly than the single layer material.

3 Control of the ESP actuator robot

ESP-based actuators are continuous actuators made of intelligent materials and are controlled differently from conventional actuators. This is due to their geometrical design and their specific actuation phenomenon.

3.1 Modeling of the ESP actuator robot

Classical robots are made up of punctual articulations linked together by rigid connections. Continuous robots, on the other hand, are made up of articulations directly integrated in their structure. They are more related to the functioning of muscles, which lengthen and contract by modifying their intrinsic structure. The major advantages of these robots are dexterity and adaptability. Yet they require specific modeling theories and are often complex to control Webster & Jones (2010), Amouri et al. (2015) and Poignet et al. (2016).

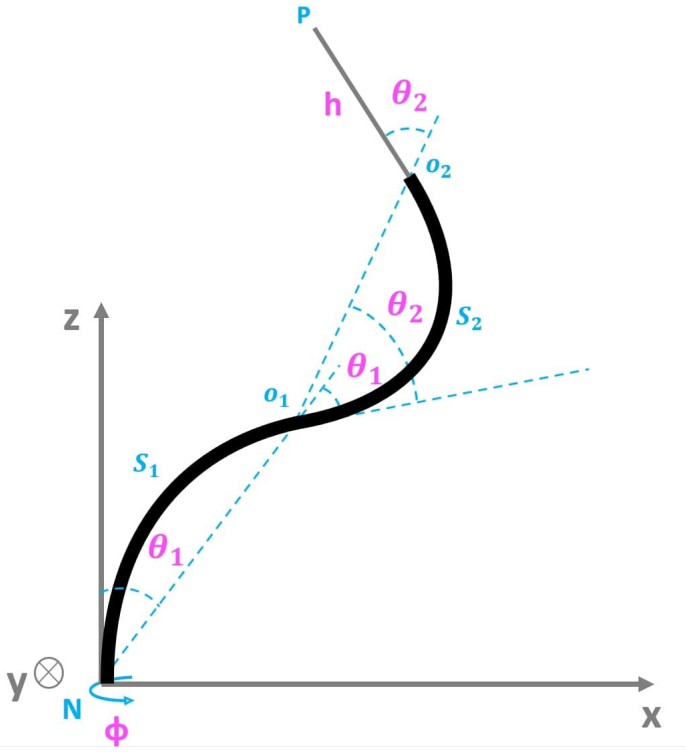

Figure 6: Parameters of the double curvature robot in ESP.

ESP actuators are subjected to a stress field and operate with large displacements at low frequency. To our knowledge, the dynamic modeling of the electrostriction phenomenon in this context has never been discussed in the literature. On the other hand, many articles describe the evolution of the dynamics of a composite material subjected to a thermal stress. Since the thermal field has a quadratic behavior in a composite material we can use this analogy to model our ESP actuator system.

Edberg (1987) and Murozono & Sumi (1994) present the control equations for flexible embedded beams through thermal fields. In particular, the thermally induced bending moment distributed over the beam is presented. This thermal moment can be described in the following equation 2:

$$M_x(t) = \int\int_A E\alpha Temp(t) z dA \tag{2}$$

Here A denotes the area of the beam, z the height and α and $Temp$ represent respectively the coefficient of thermal expansion and the temperature imposed on the material. However, they do not take into account the elastic strain in the expression of the deformation. Tuzcu & Gonzalez-Rocha (2013) and Hsueh (2002) have, on their side, studied a beam in bending under thermal loads by expressing the bending moment from the elastic and thermal effects of the material. Based on this work we developed a procedure to build a model of the electrostrictive torques of a multilayer composite material structure. The bending moment can then be written as shown in equation 3 considering the local reference frame of the actuator with the layers arranged along the thickness axis.

$$\begin{pmatrix} M_x \\ M_y \\ M_{xy} \end{pmatrix} = \sum_{i=0}^{n+1} \frac{E_i}{1-\nu_i^2} \begin{pmatrix} 1 & \nu_i & 0 \\ \nu_i & 1 & 0 \\ 0 & 0 & \frac{1-\nu_i}{2} \end{pmatrix} \int_{h(i)} \begin{pmatrix} {}^{el}\varepsilon_x^i \\ {}^{el}\varepsilon_y^i \\ \gamma_{xy}^i \end{pmatrix} z dz \tag{3}$$

$h(i)$ are the different thikness of the layers i. ${}^{el}\varepsilon_x^i$ is the elastic strain of the i layers in the x direction. The electrostrictive torque is relative to the bending of the material in the direction of

its length with $\tau_{elec} = M_x$. It can then be written as follows:

$$\tau_{elec} = \sum_{i=0}^{n+1} \left(\frac{E_i}{1-\nu_i^2} \int_{h(i)} {}^{el}\varepsilon_x^i dz + \frac{\nu_i E_i}{1-\nu_i^2} \int_{h(i)} {}^{el}\varepsilon_y^i dz \right) \tag{4}$$

with the elastic strain described in the system of equation 5. The electric field T replace the temperature and the electrostriction coefficient Mp replaces the thermal expansion coefficient α.

$$\begin{cases} {}^{el}\varepsilon_x^i(z) = \varepsilon_{0x} + zk_x - M_i T^2; & -e_s \leq z \leq n(e_e + e_p) \\ {}^{el}\varepsilon_y^i(z) = \varepsilon_{0y} + zk_y - M_i T^2; & -e_s \leq z \leq n(e_e + e_p) \end{cases} \tag{5}$$

The equation 5 is written in the local reference frame of the actuator with z in the direction of the height of the successive thicknesses of the composite material. We neglect the part in the y direction, considering that given the width of the actuators, the curvature k_y is negligible. Thus for each of the two electrostrictive actuators we obtain equation 6 describing the form of the torques formulation and with C_{ik} constant coefficients:

$$\boxed{\tau = C_{i1}k_i + C_{i2}T^2 + C_{i3} \quad i = 2,3} \tag{6}$$

The kinetic energy is written as the sum of the kinetic energies of the different robot sections, as presented by Tatlicioglu et al. (2007*b*), Tatlicioglu et al. (2007*a*) and He et al. (2013) for systems with continuous pneumatic and cable joints respectively. Based on the method proposed by He et al. and introducing the contribution of the modified Denavit-Hartenberg model, we propose a formulation for the kinetic energy. The joint space is defined by:

$$\begin{cases} q_1 = \phi \\ q_2 = k_1 \\ q_3 = k_2 \end{cases} \tag{7}$$

Thus the different sections of th e robot are defined by the points (cf figure 6):

$$\begin{cases} a_1 = N \\ a_2 = O_1 \\ a_3 = O_2 \end{cases} \tag{8}$$

The kinetic energy of the system located between the section points a_i and a_{i+1} is written as follows:

$$E_c = 1/2 \sum_i \int_{a_i}^{a_{i+1}} \left[(\frac{\partial x}{\partial t})^2 + (\frac{\partial y}{\partial t})^2 + (\frac{\partial z}{\partial t})^2 \right] \rho A ds \tag{9}$$

with ρ the density and A the area of the section. We can then develop the expression of the Cartesian coordinates in the space of the joint coordinates for each part of the system by means of the homogeneous transformation matrices from one reference frame to another. The joint coordinates for the points of the first section defined between N and O_1 are presented below:

$$\begin{cases} x = \dfrac{2 \sin\left(\frac{q_2 s}{2}\right)^2 \cos(q_1)}{q_2} \\ y = \dfrac{2 \sin\left(\frac{q_2 s}{2}\right)^2 \sin(q_1)}{q_2} \\ z = \dfrac{\sin(q_2 s)}{q_2} \end{cases} \tag{10}$$

The velocity of point O_1 can then be written in the x direction:

$$\frac{\partial x}{\partial t} = -\frac{2 \sin\left(\frac{q_2 s}{2}\right)^2 \sin(q_1)}{q_2} \frac{\partial q_1}{\partial t} + \left[-\frac{2 \sin\left(\frac{q_2 s}{2}\right) \cos(q_1) \left(\sin\left(\frac{q_2 s}{2}\right) - q_2 s \cos\left(\frac{q_2 s}{2}\right) \right)}{{q_2}^2} \right] \frac{\partial q_2}{\partial t} \tag{11}$$

In the same way we can write the kinetic energy for the section O_1O_2, E_{k2} from the joint coordinates of O_2 and the section O_2P, E_{k3} from the coordinates of the point P. We thus obtain

the total kinetic energy of the system in the form of the equation 12.

$$\boxed{E_c = \sum_{n=1}^{3} E_{cn} = \sum_{i,j} K_{i,j}(q) \frac{\partial q_i}{\partial t} \frac{\partial q_j}{\partial t} \quad i,j} \tag{12}$$

He et al. (2013) have neglected gravity energy in their work, compared to the order of magnitude of the elastic potential energy from the tension of the actuator cables in their robotic system. In this case, the gravitational potential energy integrates the contribution of the buoyancy induced by the fluid present in the robot's environment. The gravitational potential energy E_p can, again, be written as the sum of the contributions of the different parts of the robot located at the center of gravity of the z_G^i sections.

$$\begin{cases} z_G^1 = \dfrac{\sin(q_2 s)}{q_2} \\ z_G^2 = \dfrac{(q_2+q_3)\sin(q_2 s_1) - q_2 \sin(q_2 s_1 - q_3 s)}{q_2 q_3} \end{cases}$$

We thus obtain the following expression of the potential energy:

$$\boxed{E_p = \sum_i \rho_i^{tot} V_i g z_G^i \quad i = 1,2}$$

With $\rho_i^{tot} = \rho_i^{robot} - \rho_i^{fluid}$ which integrates the contribution of the buoyancy to the gravity force and V_i being the volume of the i sections of the robot. We can then develop the Lagrangian equation from the the expression of the kinetic energy and the potential energy.

$$\boxed{M_{i,i}\ddot{q}_i + C_{i,i}\dot{q}_i^2 + B_{i,i}\dot{q}_i\dot{q}_j + G_i = \dot{q}_j} \tag{13}$$

We obtain the dynamic model in equation 13 where M is the inertia matrix, the matrix of the effects of the centrifugal force $C(q)$, the Coriolis force $B(q)$ and the effects of the conservative forces (gravity force and buoyancy) $G(q)$.

3.2 Design of a cosimulation model to simulate the ESP actuator robot control

In order to validate the modeling of the robot and to observe its dynamic behavior under control theories, we developed a multiphysic virtual model presented in figure 7 divided on three programming environments, Matlab, Simulink and Abaqus.

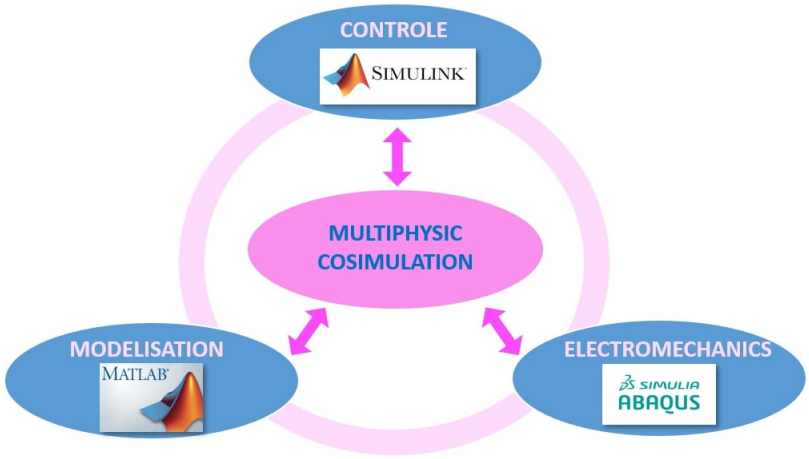

Figure 7: Multiphysics cosimulation structure diagram

The three-actuator Abaqus model is shown in figure 8. The ESP actuators are located after the rotating base of the system. They measure respectively 40mm and 10mm. A separation of 0.2mm of passive material has been inserted between the two continuous joints as an isolation to avoid thermal coupling. The distal part of the robot can now be controlled in flexion and deflection. The rotating base is made from a steel cube, for which only rotation is allowed. The mesh size is reduced at the embedded junction between the first actuator and the cube in order to not constrain the strain of the first embedded elements. Finally, we have developed a nonlinear geometric model and the analysis is performed under the implicit dynamic mode.

The virtual robot model in cosimulation is controlled in this section by a PID (Propor-

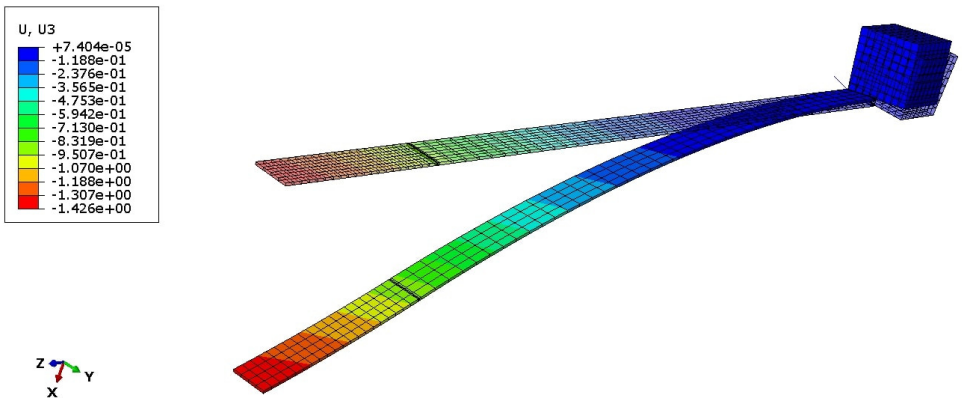

Figure 8: Abaqus finite element model of the three actuator system

tional Integral Derivative) controller with a gain $G(s) = K_P + K_I.\frac{1}{s} + K_D.s$. The following simulation presents the variation of the robot head for a slot setpoint with an open loop system and a closed loop system (figure 9). The loop is closed by the comparison between abaqus position feedback and the expected position. We can again observe that the PID controller

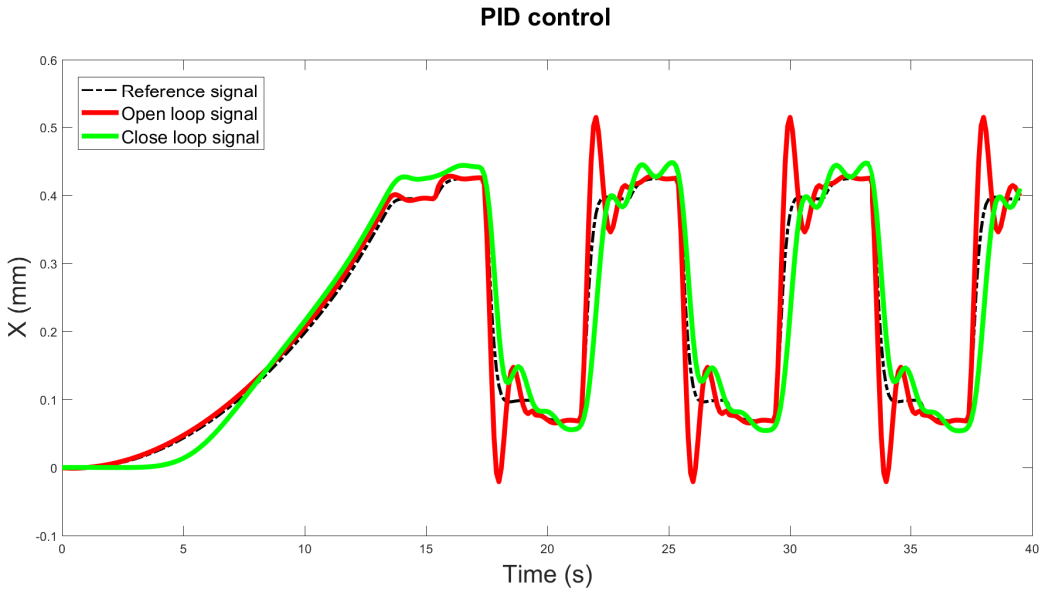

Figure 9: Robot PID control results

works correctly although a delay can be observed between the set point and the signal. This

is due to feedback stability issues. Indeed it is related to the difficulty to increase the gain K_D without accentuating the dynamic effects and thus destabilizing the robot. To cope with this problem, we have proose a new control strategy base on the use of dynamic anticipation term. Hence, besed on the dynamical model developed previously, we ha added an anticipation term that will tend to compensate these effects as presented in figure 10a. Figure 10b shows the cosimulation result of the three-actuator robot tracking a reference trajectory extract from a previous open loop simulation. We observe in this figure that the PID signal with the dynamic feedforward term reduces the static error. Despite this, the rise time is still large and some overshoots cannot be corrected. The effects of the material stiffness would have to be taken into account to fully compensate the irregularities related to the step changes.

4 Discussion

The electrostrictive polymer showed good bending capabilities during the experimental tests. However, it is clear that the control of the printing process is essential for the realization of efficient actuators. Therefore, a theoretical study of the influence of the different steps of the printing process and especially of the annealing on the reorganization of the material crystalline structure, would have been relevant and deserves to be the subject of future research Bargain et al. (2021). In addition, the evaluation of other techniques such as dip coating could open the way to the realization of actuators of different geometries. A cylindrical actuator has been studied by Ganet et al. (2016). This new actuator would again be guided by its numerical twin developed on Abaqus. A molecular scale study of the interaction of the layers, depending on the printing process, could also be conducted and then integrated into the numerical model. Indeed, the bending process depends precisely on the junction between the passive substrate and the block constituted by the electrodes and the electroactive polymer. Similarly, in the case of multilayer actuators, the role of the passive substrate is amplified by each of the active layers preceding the layer under study.

The numerical model then evolved towards a consideration of the complete structure of the robot. This model deserves to be improved by integrating the torsional constraints resulting

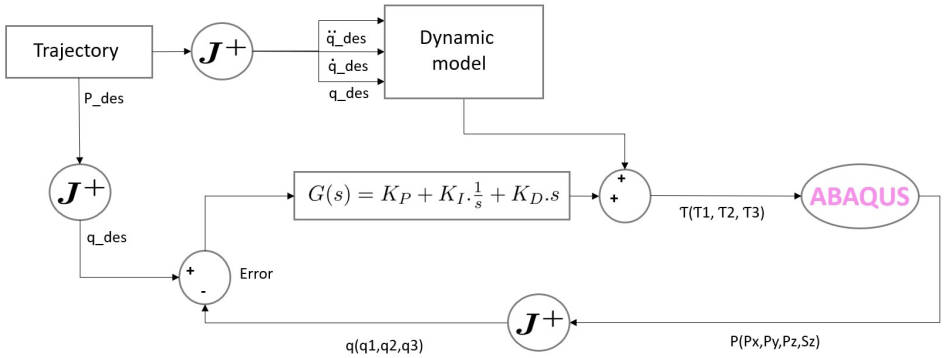

(a)

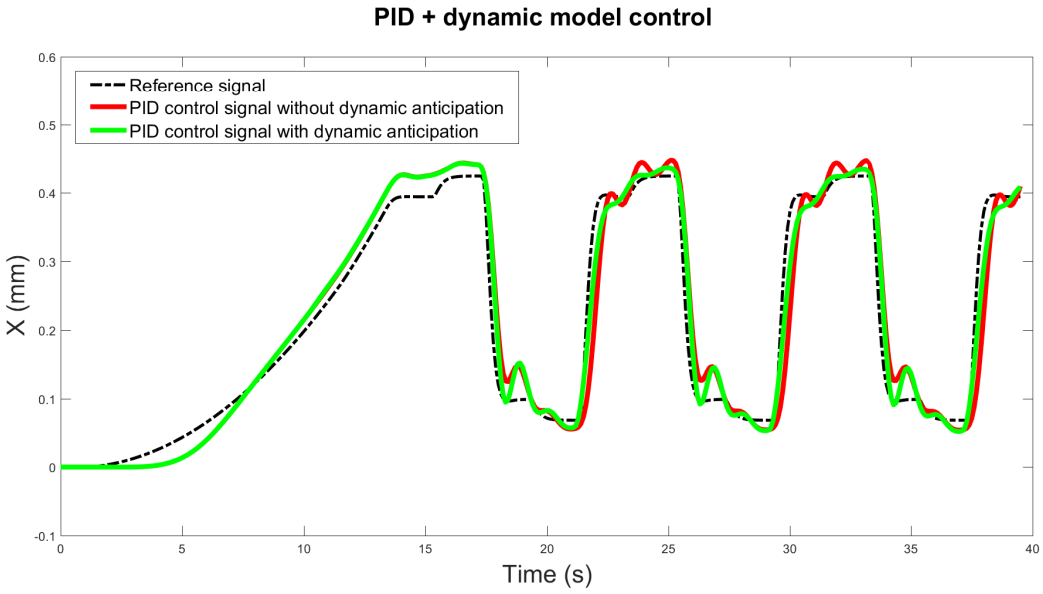

(b)

Figure 10: a) Schematic of the PID controller with dynamic anticipation and b) Robot PID control results with and without the dynamic feedforward terms

from the rotation of the robot base as well as the loading of the embedded equipment. The dynamic model developed in this article must also evolve in order to take the environmental constraints into account and thus allow the development of control algorithm adapted to the challenges of such surgical robots.

5 Conclusion

ESP continuum actuators for MIS applications have shown great interest for their bending capacities and direct integration. yet the fabrication process and the composite material parameters had to be improved. After highlighting the ability of the different parameters to generate bending and induced force, we were able to guide the experimental process towards the design of a high-performance actuator for our application and for micro robotics in general. This experimental study confirmed some of the hypotheses raised by the theoretical model while highlighting the difficulty of realizing an actuator free of manufacturing defects. These results demonstrated the bending capabilities of this continuous joint made of smart material since an angle of more than 180° was reached while showing a capacity of repeatability, reversibility and precision. However, the force values obtained are not yet up to the expectations of such an actuator. Thus, new manufacturing techniques towards the realization of multilayer materials must be explored. The problem of high actuation voltage was solved by the multilayer solution. This was proven by numerical analysis and while a multilayer actuator was not experimentally printed, a bilayer actuator was successfully printed, showing the expected behavior and thus paving the way for multilayer design.

Continuous smart materials actuators modeling differs from the traditional theories developed for rigid robots with punctual joints. We established in this article the geometric, kinematic and dynamic models This model was later validated on a digital twin developed in co-simulation on Matlab, Simulink and Abaqus software. Through a control model by PID corrector, we have validated the theoretical model proposed in this work. This digital twin will enable to test and validate more control theories in the robot in the futur.

5.1 ACKNOWLEDGMENT

This research was supported by Piezotech S.A.S (Arkema group, France), Laboratoires Coloplast (Coloplast group, Denmark) and Tenon Hospital Urology service (France). Sylvie Tencé-Girault's contribution was achieved within the framework of the Industrial Chair Arkema (Arkema/CNRS-ENSAM-CNAM).

References

Ahmed, M. & Billah, M. M. (2016), 'Smart Material-Actuated Flexible Tendon-Based Snake Robot', *International Journal of Advanced Robotic Systems* **13**(3), 89.
URL: http://journals.sagepub.com/doi/10.5772/62187

Ahmed, S., Ounaies, Z. & Arrojado, E. A. F. (2017), 'Electric field-induced bending and folding of polymer sheets', *Sensors and Actuators A: Physical* **260**, 68–80.
URL: https://linkinghub.elsevier.com/retrieve/pii/S0924424717304594

Amouri, A., Mahfoudi, C. & Zaatri, A. (2015), 'Modélisation d'une classe des robots flexibles bio-inspirés a courbure constante', . *Constantine* p. 10.

Balakrisnan, B., Nacev, A. & Smela, E. (2015), 'Design of bending multi-layer electroactive polymer actuators', *Smart Materials and Structures* **24**(4), 045032.
URL: https://iopscience.iop.org/article/10.1088/0964-1726/24/4/045032

Bar-Cohen, Y. (2004*a*), EAP as artificial muscles: progress and challenges, San Diego, CA, p. 10.
URL: http://proceedings.spiedigitallibrary.org/proceeding.aspxdoi=10.1117/12.538698

Bar-Cohen, Y. (2004*b*), Electroactive polymers (EAP) as actuators for potential future planetary mechanisms, *in* 'Proceedings. 2004 NASA/DoD Conference on Evolvable Hardware, 2004.',

IEEE, Seattle, WA, USA, pp. 309–317.
URL: http://ieeexplore.ieee.org/document/1310845/

Bargain, F., Thuau, D., Hadziioannou, G., Domingues Dos Santos, F. & Tencé-Girault, S. (2021), 'Phase diagram of poly(VDF-ter-TrFE-ter-CTFE) copolymers: Relationship between crystalline structure and material properties', *Polymer* **213**, 123203.
URL: https://linkinghub.elsevier.com/retrieve/pii/S0032386120310284

Capsal, J.-F., Galineau, J., Le, M.-Q., Domingues Dos Santos, F. & Cottinet, P.-J. (2015), 'Enhanced electrostriction based on plasticized relaxor ferroelectric P(VDF-TrFE-CFE/CTFE) blends', *Journal of Polymer Science Part B: Polymer Physics* **53**(19), 1368–1379.
URL: http://doi.wiley.com/10.1002/polb.23776

Cho, Y., Ahn, D., Park, J. B., Pak, S., Lee, S., Jun, B. O., Hong, J., Lee, S. Y., Jang, J. E., Hong, J., Morris, S. M., Sohn, J. I., Cha, S. N. & Kim, J. M. (2016), 'Enhanced Ferroelectric Property of P(VDF-TrFE-CTFE) Film Using Room-Temperature Crystallization for High-Performance Ferroelectric Device Applications', *Advanced Electronic Materials* **2**(10), 1600225.
URL: http://doi.wiley.com/10.1002/aelm.201600225

Duduta, M., Wood, R. J. & Clarke, D. R. (2016), 'Multilayer Dielectric Elastomers for Fast, Programmable Actuation without Prestretch', *Advanced Materials* **28**(36), 8058–8063.
URL: https://onlinelibrary.wiley.com/doi/10.1002/adma.201601842

Edberg, D. L. (1987), 'Control of flexible structures by applied thermal gradients', *AIAA Journal* **25**(6), 877–883.
URL: https://arc.aiaa.org/doi/10.2514/3.9715

Frecker, M. I. & Aguilera, W. M. (2004), 'Analytical modeling of a segmented unimorph actuator using electrostrictive P(VDF-TrFE) copolymer', *Smart Materials and Structures* **13**(1), 82–91.

URL: http://stacks.iop.org/0964-1726/13/i=1/a=010key=crossref.7fff2428eed254e69494ae8f1169c642

Ganet, F., Le, M. Q., Capsal, J. F., Lermusiaux, P., Petit, L., Millon, A. & Cottinet, P. J. (2016), 'Development of a smart guide wire using an electrostrictive polymer: option for steerable orientation and force feedback', *Scientific Reports* **5**(1).
URL: http://www.nature.com/articles/srep18593

He, B., Wang, Z., Li, Q., Xie, H. & Shen, R. (2013), 'An Analytic Method for the Kinematics and Dynamics of a Multiple-Backbone Continuum Robot', *International Journal of Advanced Robotic Systems* **10**(1), 84.
URL: http://journals.sagepub.com/doi/10.5772/54051

Hsueh, C. (2002), 'Thermal stresses in elastic multilayer systems', *Thin Solid Films* **418**(2), 182–188.
URL: http://linkinghub.elsevier.com/retrieve/pii/S0040609002006995

Kadooka, K., Taya, M., Naito, K. & Saito, M. (2015), Modeling of a corrugated dielectric elastomer actuator for artificial muscle applications, San Diego, California, United States, p. 943020.
URL: http://proceedings.spiedigitallibrary.org/proceeding.aspxdoi=10.1117/12.2084733

Kant, T., Arora, C. & Varaiya, J. (1992), 'Finite element transient analysis of composite and sandwich plates based on a refined theory and a mode superposition method', *Composite Structures* **22**(2), 109–120.
URL: https://linkinghub.elsevier.com/retrieve/pii/026382239290071J

Lheritier, P., Vaxelaire, N., Tencé-Girault, S., Domingues Dos Santos, F. & Defay, E. (2020), 'Influence of Field-Induced Phase Transition on Poly(Vinylidene Fluoride-Trifluoroethylene-

Chlorotrifluoroethylene) Strain', *Physical Review Applied* **14**(4), 044061.
URL: https://link.aps.org/doi/10.1103/PhysRevApplied.14.044061

McGough, K., Ahmed, S., Frecker, M. & Ounaies, Z. (2014), 'Finite element analysis and validation of dielectric elastomer actuators used for active origami', *Smart Materials and Structures* **23**(9), 094002.
URL: https://iopscience.iop.org/article/10.1088/0964-1726/23/9/094002

Murozono, M. & Sumi, S. (1994), 'Active Vibration Control of a Flexible Cantilever Beam by Applying Thermal Bending Moment', *Journal of Intelligent Material Systems and Structures* **5**(1), 21–29.
URL: http://journals.sagepub.com/doi/10.1177/1045389X9400500103

O'Brien, B., Calius, E., Xie, S. & Anderson, I. (2008), An experimentally validated model of a dielectric elastomer bending actuator, San Diego, California, p. 69270T.
URL: http://proceedings.spiedigitallibrary.org/proceeding.aspxdoi=10.1117/12.776098

Pandya, B. N. & Kant, T. (1988), 'Finite Element Analysis of Laminated Composite Plates using a Higher-Order Displacement Model', p. 19.

Poignet, P., Szewczyk, J., Cattan, É., Renaud, P., Rabenorosoa, K. & Andreff, N. (2016), 'Nouveau concept de robots à tubes concentriques à micro-actionneurs à base de polymères électro-actifs', p. 269.

Tatlicioglu, E., Walker, I. D. & Dawson, D. M. (2007*a*), New dynamic models for planar extensible continuum robot manipulators, *in* '2007 IEEE/RSJ International Conference on Intelligent Robots and Systems', IEEE, San Diego, CA, USA, pp. 1485–1490.
URL: http://ieeexplore.ieee.org/document/4399334/

Tatlicioglu, E., Walker, I. & Dawson, D. (2007*b*), 'Dynamic Modelling for Planar Extensible Continuum Robot Manipulators', *Proceedings 2007 IEEE International Conference on Robotics and Automation* p. 6.

Tuzcu, I. & Gonzalez-Rocha, J. (2013), Modeling and Control of a Thermoelastic Beam, *in* 'Volume 1: Aerial Vehicles; Aerospace Control; Alternative Energy; Automotive Control Systems; Battery Systems; Beams and Flexible Structures; Biologically-Inspired Control and its Applications; Bio-Medical and Bio-Mechanical Systems; Biomedical Robots and Rehab; Bipeds and Locomotion; Control Design Methods for Adv. Powertrain Systems and Components; Control of Adv. Combustion Engines, Building Energy Systems, Mechanical Systems; Control, Monitoring, and Energy Harvesting of Vibratory Systems', American Society of Mechanical Engineers, Palo Alto, California, USA.
URL: https://asmedigitalcollection.asme.org/DSCC/proceedings/DSCC2013/56123/Palo%20Alto,%20California,%20USA/228661

Webster, R. J. & Jones, B. A. (2010), 'Design and Kinematic Modeling of Constant Curvature Continuum Robots: A Review', *The International Journal of Robotics Research* **29**(13), 1661–1683.
URL: http://journals.sagepub.com/doi/10.1177/0278364910368147